

PRTGS: Precomputed Radiance Transfer of Gaussian Splats for Real-Time High-Quality Relighting

Yijia Guo
State Key Laboratory of
Multimedia Information
Processing, School of
Computer Science, Peking
University
Beijing, China
2301112015@stu.pku.edu.cn

Yuanxi Bai
College of Future
Technology, Peking
University
Beijing, China
2301210592@stu.pku.edu.cn

Liwen Hu
State Key Laboratory of
Multimedia Information
Processing, School of
Computer Science, Peking
University
Beijing, China
huliwen@pku.edu.cn

Ziyi Guo
College of Future
Technology, Peking
University
Beijing, China
guoziyi1123@stu.pku.edu.cn

Mianzhi Liu
College of Future
Technology, Peking
University
Beijing, China
liumianzhi@stu.pku.edu.cn

Yu Cai
College of Future
Technology, Peking
University
Beijing, China
2406799035@pku.edu.cn

Tiejun Huang
State Key Laboratory of
Multimedia Information
Processing, School of
Computer Science, Peking
University
Beijing, China
tjhuang@pku.edu.cn

Lei Ma*
State Key Laboratory of
Multimedia Information
Processing, School of
Computer Science, Peking
University
Beijing, China
lei.ma@pku.edu.cn

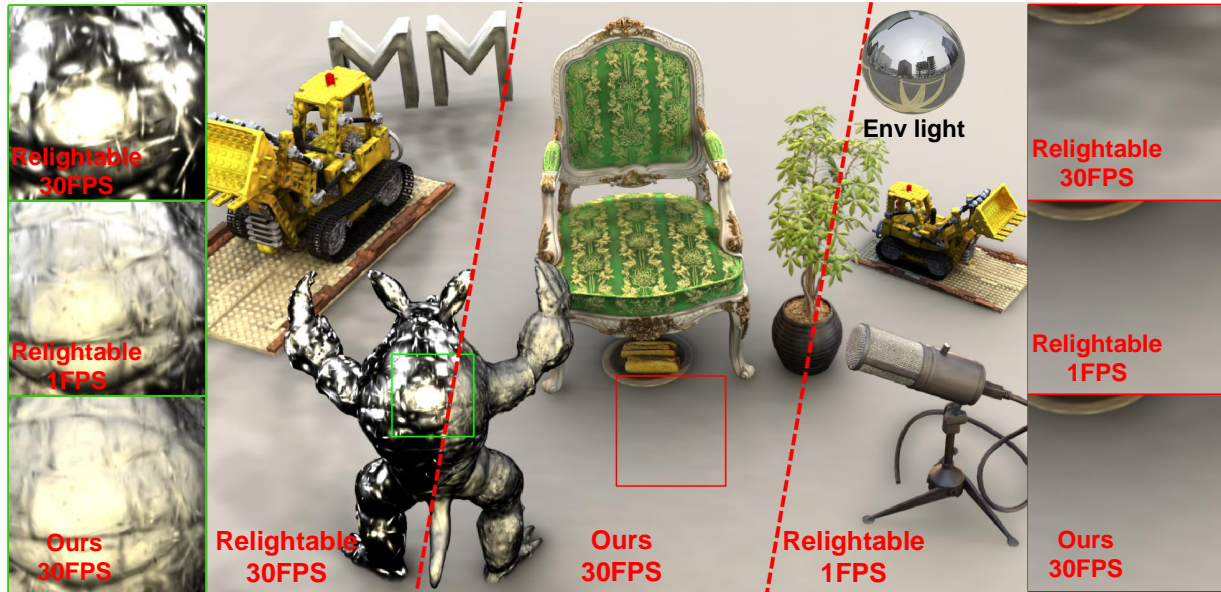


Figure 1: An edited complex scene with over 1000000 Gaussian splats relighted by dynamic lights. (Right) Offline result (less than 1 FPS) from Relightable 3DGS [7]. (Middle) Real-time results conducted by our PRGS. (Left) Real-time results from Relightable 3DGS. All methods run equally on a Nvidia RTX 3090 GPU. Note that for comparable rendering times to the current real-time relighting method, we achieve similar quality to their offline rendering results.

* Corresponding author.

This work was supported by National Science and Technology Major Project (2022ZD0116305).

Permission to make digital or hard copies of all or part of this work for personal or classroom use is granted without fee provided that copies are not made or distributed for profit or commercial advantage and that copies bear this notice and the full citation on the first page. Copyrights for components of this work owned by others than the author(s) must be honored. Abstracting with credit is permitted. To copy otherwise, or republish, to post on servers or to redistribute to lists, requires prior specific permission and/or a fee. Request permissions from permissions@acm.org.

MM'24, October 28 - November 1, 2024, Melbourne, Australia.

ABSTRACT

We proposed Precomputed Radiance Transfer of Gaussian Splats (PRTGS), a real-time high-quality relighting method for Gaussian splats in low-frequency lighting environments that captures soft shadows and interreflections by precomputing 3D Gaussian splats' radiance transfer. Existing studies have demonstrated that

© 2024 Copyright held by the owner/author(s). Publication rights licensed to ACM.
ACM ISBN 979-8-4007-0686-8/24/10...\$15.00
<https://doi.org/10.1145/3664647.3680893>

3D Gaussian splatting (3DGS) outperforms neural fields' efficiency for dynamic lighting scenarios. However, the current relighting method based on 3DGS is still struggling to compute high-quality shadow and indirect illumination in real time for dynamic light, leading to unrealistic rendering results. We solve this problem by precomputing the expensive transport simulations required for complex transfer functions like shadowing, the resulting transfer functions are represented as dense sets of vectors or matrices for every Gaussian splat. We introduce distinct precomputing methods tailored for training and rendering stages, along with unique ray tracing and indirect lighting precomputation techniques for 3D Gaussian splats to accelerate training speed and compute accurate indirect lighting related to environment light. Experimental analyses demonstrate that our approach achieves state-of-the-art visual quality while maintaining competitive training times and allows high-quality real-time (30+ fps) relighting for dynamic light and relatively complex scenes at 1080p resolution.

CCS CONCEPTS

• **Computing methodologies** → **Rendering; Ray tracing; Point-based models; Machine learning algorithms.**

KEYWORDS

Precomputed Radiance Transfer, Radiance Field, 3D Gaussian Splatting, Relighting

ACM Reference Format:

Yijia Guo, Yuanxi Bai, Liwen Hu, Ziyi Guo, Mianzhi Liu, Yu Cai, Tiejun Huang, and Lei Ma*. 2024. PRTGS: Precomputed Radiance Transfer of Gaussian Splats for Real-Time High-Quality Relighting. In *Proceedings of Make sure to enter the correct conference title from your rights confirmation email (MM'24)*. ACM, New York, NY, USA, 9 pages. <https://doi.org/10.1145/3664647.3680893>

1 INTRODUCTION

3D Gaussian Splatting [11] has garnered significant attention from the community as a promising approach for various tasks in 3D scene reconstruction. The utilization of 3DGS presents the potential for individuals to reconstruct their surrounding environment using contemporary technological devices such as smartphones and computers in minutes. Furthermore, individuals can modify their reconstructed world according to their unique preferences, which makes it particularly attractive for multimedia applications and could potentially spur innovation within the multimedia industry. The foundation for achieving this lies in a real-time and high-quality inverse rendering, relighting, and scene editing method.

The achievement of real-time inverse rendering and relighting has been a long-standing problem. Methods based on Neural Radiance Fields (NeRF) [9, 20, 37] have exhibited noteworthy accomplishments in high-quality material editing, illumination computing, and shadow estimation. However, these techniques struggle with the computational overhead and cannot achieve the desired quality in dynamic environmental lighting conditions. The integration of MLPs within these methods gives rise to inherent obstacles owing to their restricted expressive capacity and substantial computational demands. These obstacles engender a considerable curtailment of the effectiveness and efficiency of inverse rendering. Current works

[7, 16, 27] introduce 3DGS to inverse rendering instead of NeRF, achieving high-performance inverse rendering and relighting by employing a set of 3D Gaussian splats to represent a 3D scene. However, they still face challenges in the real-time computation of high-quality indirect lighting and shadows in dynamic environmental lighting conditions, primarily due to the utilization of ray tracing or ambient occlusion techniques. The former struggles with balancing quality and speed because of the immense number of Gaussian splats involved [7], while the latter have difficulty in computing realistic indirect lighting [16].

In this paper, we solve the aforementioned challenge by introducing Precomputed Radiance Transfer (PRT) [28] to 3DGS. Starting with assigning each 3D Gaussian splat with normal (geometry), visibility, and BRDF attributes, we precompute the expensive transport simulation required by complex transfer functions like shadowing and interreflection for given 3d Gaussian splats. The precomputed transfer functions and incident radiance are encoded as either a dense set of vectors (diffuse cases) or matrices (glossy cases), utilizing a low-order spherical harmonic (SH) basis for each Gaussian splats distribution. This approach allows for an efficient representation of the complex transfer functions while maintaining a high level of accuracy. Leveraging the linearity inherent in light transport, we streamline the light integration process to a straightforward dot product operation between their coefficient vectors for diffuse surfaces, or a compact transfer matrix for glossy surfaces, significantly reducing computational overhead.

Our approach not only enhances real-time rendering quality in dynamic lighting but also opens up new possibilities for interactive multimedia applications. We developed unique precomputing and ray tracing methods that are specifically tailored to accommodate the unique geometry and rendering pipeline of 3DGS. This ensures that our approach is optimized to provide high-quality results while maintaining computational efficiency. Specifically, during the training stage, we carefully designed different reflection strategies for various surfaces under different conditions, ensuring the quality of interreflection while significantly reducing training time. Our unique ray tracing method allows us to perform only one-bounce ray tracing throughout the whole training or testing stage, resulting in real-time photorealistic rendering results. Extensive experimental analyses have demonstrated that our proposed approach significantly outperforms existing methods on synthetic and real-world datasets across multiple tasks. We summarize our main contributions as follows:

- We applied PRT to 3DGS for the first time, achieving high-quality real-time relighting in complex scenes under dynamic lighting conditions, while also supporting high-quality scene editing.
- For efficiency, we designed distinct precomputing methods for both training and rendering stage. Additionally, we devised unique ray tracing and indirect lighting precomputation methods for 3DGS to accelerate training speed and compute accurate indirect illumination related to environmental lighting.
- Through comprehensive experimentation, we have demonstrated that our approach outperforms relevant schemes. The experimental results highlight that our method not only

facilitates high-quality real-time relighting but also excels in supporting high-quality scene editing.

2 RELATED WORK

2.1 Radiance Fields

Neural Radiance Field (NeRF) [18] has arisen as a significant development in the field of Computer Vision and Computer Graphics, used for synthesizing novel views of a scene from a sparse set of images by combining machine learning with geometric reasoning. Recently, a plethora of research and methodologies built upon NeRF have been proposed. For example, [15, 22, 23, 31] extend NeRF to dynamic and non-grid scenes, [2, 3] significantly improve the rendering quality of NeRF. Recently, researchers have collectively recognized that the bottleneck in efficiency lies in querying the neural field, prompting efforts to address it. InstantNGP [19] combines a neural network with a multiresolution hash table for efficient evaluation while Plenoxels [6] replaces neural networks with a sparse voxel grid. 3D Gaussian splatting [11] further adopts a discrete 3D Gaussian representation of scenes, significantly accelerating the training and rendering of radiance fields. It has attracted considerable research interest in the field of generation [5, 34], relighting [7, 16, 27] and dynamic 3D scene reconstruction [30, 32].

2.2 Relighting and Inverse Rendering

Inverse rendering [25, 26] aims to decompose the image's appearance into the geometry, material properties, and lighting conditions. Most traditional methods simplified the problem by assuming controllable lighting conditions [1, 35]. Works based on Nerf explore more complex lighting models to cope with realistic scenarios and extensively utilize MLPs to encode lighting and materials properties. NeRV [29] and Invrender [38] train an additional MLP to model the light visibility. NeILF [33] expresses the incident lights as a neural incident light field. NeILF++ [36] integrates VolSDF with NeILF and unifies incident light and outgoing radiance. TensorIR [9] introduces TensorRF representation which enables the computation of visibility and indirect lighting by raytracing. Works based on 3DGS [7, 16, 27] have significantly accelerated training and rendering, enabling real-time relighting and editing. However, these methods still face challenges in real-time high-quality indirect lighting computation, dynamic relighting, and shadow estimation.

2.3 Precompute Radiance Transfer

The fundamental concept of Precompute Radiance Transfer (PRT) [28] involves selecting an angular basis comprised of continuous functions, notably Spherical Harmonics (SH), and conducting all light transport operations within this domain. However, Spherical Harmonics are limited in terms of high frequencies, Sloan [17] then replace it with Haar wavelet. Kristensen [12] further extends PRT to local lighting and pan [21] extends it to dynamic scenes. Recently there has been a growing interest in using deep learning tools within traditional PRT frameworks [14, 24], and ideas from PRT have been used in the context of the radiance field [13].

3 PRELIMINARY

3.1 3D Gaussian splatting

Distinct from the widely adopted Neural Radiance Field, 3D Gaussian Splatting is an explicit 3D scene representation in the form of point clouds, where Gaussian splats are utilized to represent the structure of the scene. In this representation, every Gaussian splat G is defined by a full 3D covariance matrix Σ as well as the center (mean) $x \in \mathbb{R}^3$.

$$G(x) = e^{-1/2(x)^T \Sigma^{-1}(x)} \quad (1)$$

The covariance matrix Σ of a 3D Gaussian splat can be likened to characterizing the shape of an ellipsoid. Therefore, we can describe it using a rotation matrix R and a scale matrix S and independently optimize of both them.

$$\Sigma = RSS^T R^T \quad (2)$$

To project our 3D Gaussian splats to 2D for rendering, the method of splatting is utilized for positioning the Gaussian splats on the camera planes:

$$\Sigma' = J W \Sigma W^T J^T \quad (3)$$

Where J is the Jacobian of the affine approximation of the projective transformation and W is the viewing transformation. Following this, the pixel color is obtained by alpha-blending N sequentially layered 2D Gaussian splats from front to back:

$$C = \sum_{i \in N} c_i \alpha_i \prod_{j=1}^{i-1} (1 - \alpha_j) \quad (4)$$

Where c_i is the color of each point and α_i is given by evaluating a 2D Gaussian with covariance Σ multiplied with a learned per-point opacity.

3.2 Precompute Radiance Transfer

According to [10], the outgoing radiance L_o at a point x with normal n observed by the camera in direction ω_o is given by the Rendering Equation:

$$L_o(\omega_o, x) = L_e + \int_{\Omega} f(x, \omega_i, \omega_o) L_i(\omega_i, x) (\omega_i, n) V(\omega_i, x) d\omega_i \quad (5)$$

where L_i corresponds to the incident light coming from direction ω_i , and $f(x, \omega_i, \omega_o)$ represents the Bidirectional Reflectance Distribution Function (BRDF) properties of the point corresponding to ω_i and outgoing direction ω_o . If we assume that objects in the scene do not have self-emission. Further, we have:

$$L_o(\omega_o, x) = \int_{\Omega} T(x, \omega_i, \omega_o) L_i(\omega_i \cdot x) d\omega_i \quad (6)$$

where

$$T(x, \omega_i, \omega_o) = f(x, \omega_i, \omega_o) (\omega_i \cdot n) V(\omega_i, x) \quad (7)$$

corresponds to the radiance transfer. Our goal is to precompute incident light L_i and radiance transfer T and project them into SH domain. According to [28], any function $F(s)$ defined on the sphere S can be represented as a set of SH basis functions:

$$F(s) = \sum_{l=0}^{n-1} \sum_{m=-l}^l f_l^m Y_l^m(s) \quad (8)$$

where n denotes the degree of SH and $Y_l^m(s)$ is a set of real basis of SH. Because the SH basis is orthonormal, the scalar function F can be projected into its coefficients via the integral:

$$f_l^m = \int F(s) Y_l^m(s) ds \quad (9)$$

Then, $L_i(\omega_i)$ at x defined on ω_i can be represented as:

$$L_i(\omega_i) = \sum_{l=0}^{n-1} \sum_{m=-l}^l l_l^m Y_l^m(\omega_i) = \sum_{j=1}^{n^2} l_j Y_j(\omega_i) \quad (10)$$

and for diffuse cases, $f(x, \omega_i, \omega_o) = \rho/\pi$ which is not related to ω_o , we have:

$$T_i(\omega) = \sum_{l=0}^{n-1} \sum_{m=-l}^l t_l^m Y_l^m(\omega_i) = \sum_{j=1}^{n^2} t_j Y_j(\omega_i) \quad (11)$$

Because T is also defined only on ω_i . Equation 5 can be written as:

$$L_o(x) = \sum_{p=1}^{n^2} \sum_{q=1}^{n^2} l_p t_q \int_{\Omega} Y_p(\omega_i) Y_q(\omega_i) d\omega_i \quad (12)$$

Considering:

$$\int_{\Omega} Y_p(\omega_i) Y_q(\omega_i) d\omega_i = \begin{cases} 1 & \text{if } q = p \\ 0 & \text{otherwise} \end{cases} \quad (13)$$

Then equation 12 can be written as:

$$L_o(x) = \sum_{i=0}^{n^2} l_i t_i = \vec{L} \cdot \vec{T} \quad (14)$$

where $\vec{T} = \{t_1, \dots, t_{n^2}\}$ and $\vec{L} = \{l_1, \dots, l_{n^2}\}$. In summary, we can project the lighting and radiance transfer to the basis to obtain \vec{L} and \vec{T} . Rendering at each point is reduced to a dot product. For glossy cases, light transport will be obtained as a transfer matrix. Please refer to sec 4.5 and supplementary for more details.

4 METHOD

4.1 Overview

In this section, we present our precomputed Gaussian splats radiance transfer framework, shown in Fig 2, which decomposes geometry, materials, and illumination for Gaussian splats (sec 4.2 and 4.3). In addition, we developed unique precomputing and ray tracing methods that are specifically tailored to accommodate the unique geometry and rendering pipeline of 3DGS (sec 4.4). Finally, we recursively compute self-transfer and project radiance transfer into SH coefficients for fast rendering (sec 4.5).

4.2 BRDF Rendering

To facilitate the physically based rendering of 3D Gaussian splats, we introduce a parametrization scheme that includes an additional set of terms for optimization purposes, *i.e.* albedo $\rho \in [0, 1]$, roughness $r \in [0, 1]$ and metallic $m \in [0, 1]$. According to Disney BRDF model [4], the BRDF property $f(\omega_i, \omega_o)$ of a material can be decomposed into two components: roughness BRDF f_d and specular BRDF f_s .

$$f(\omega_i, \omega_o) = (1 - m) \frac{\rho}{\pi} + \frac{DFG}{4(\omega_i \cdot n)(\omega_o \cdot n)} = f_d + f_s \quad (15)$$

where D is the microfacet distribution function, F is the Fresnel reflection and G is the geometric shadowing factor all of which are related to the roughness r . Then equation 5 can be written as:

$$L_o(\omega_o) = L_o^s(\omega_o) + L_o^d \quad (16)$$

where:

$$L_o^d = f_d \int_{\Omega} L_i(\omega_i, x)(\omega_i, n) d\omega_i \quad (17)$$

$$L_o^s(\omega_o) = \int_{\Omega} f_s(x, \omega_i, \omega_o) L_i(\omega_i, x)(\omega_i, n) d\omega_i \quad (18)$$

4.3 Lighting and Geometry Modeling

Lighting Modeling The majority of existing methods decompose the incident light L_i at point x into two components: direct illumination L_i^{dir} and indirect illumination L_i^{in} . Equation 6 can be further written as:

$$L_o(\omega_o) = \int_{\Omega} T(\omega_i, \omega_o) (L_i^{dir}(\omega_i) + (L_i^{in}(\omega_i))) d\omega_i \quad (19)$$

However, computing accurate indirect illumination in real-time for 3D Gaussian splats is a challenging task. We precompute self-transfer instead of directly computing indirect illumination. Considering:

$$L_i^{in}(-\omega_i) = \int_{\Omega} T^1(\omega_i^1, -\omega_i) (L_i^{dir}(\omega_i^1) + (L_i^{in}(\omega_i^1))) d\omega_i^1 \quad (20)$$

where $T^1(\omega_i^1, -\omega_i)$ is the light transfer at point (splat) x^1 which is hit by one-bounce ray tracing. Recursively, we have:

$$L_o(\omega_o) = \int_{\Omega} T'(\omega_i, \omega_o) L_i^{dir}(\omega_i) d\omega_i \quad (21)$$

where

$$T'(\omega_i, \omega_o) = T(\omega_i, \omega_o) + T(\omega_i, \omega_o) \int_{\Omega} T^1(\omega_i^1, -\omega_i) d\omega_i^1 \quad (22)$$

$$+ \dots + T(\omega_i, \omega_o) \int_{\Omega} \dots \int_{\Omega} T^n(\omega_i^n, -\omega_i^{n-1}) d\omega_i^n$$

and the global direct light term L_{dir} is parameterized as a globally shared SH, denoted as l_{dir} , and indirect light is represented as the direct light multiplied by self-transfer.

Geometry Modeling Same as [7, 9, 16, 37], we utilize the depth gradient to derive pseudo-normals, which in turn serve as guidance for optimizing normals within the 3D Gaussian splats. Given the distance from the corresponding 3D Gaussian splat to the image plane d_i and the α_i by evaluating a 2D Gaussian with covariance Σ multiplied with a learned per-point opacity, we obtain pseudo depth D derived from equation 4:

$$D = \sum_{i \in N} d_i \alpha_i \prod_{j=1}^{i-1} (1 - \alpha_j) \quad (23)$$

The pseudo-normal $N' \in HxW$ can be computed from D . However, calculating the normal n_i for each Gaussian from N through interpolation is highly inaccurate. Therefore, like [7, 9], we initialize a random normal n_i for each Gaussian splat and constrain it using normal loss L_{normal} . Here:

$$L_{normal} = \|N - N'\| \quad (24)$$

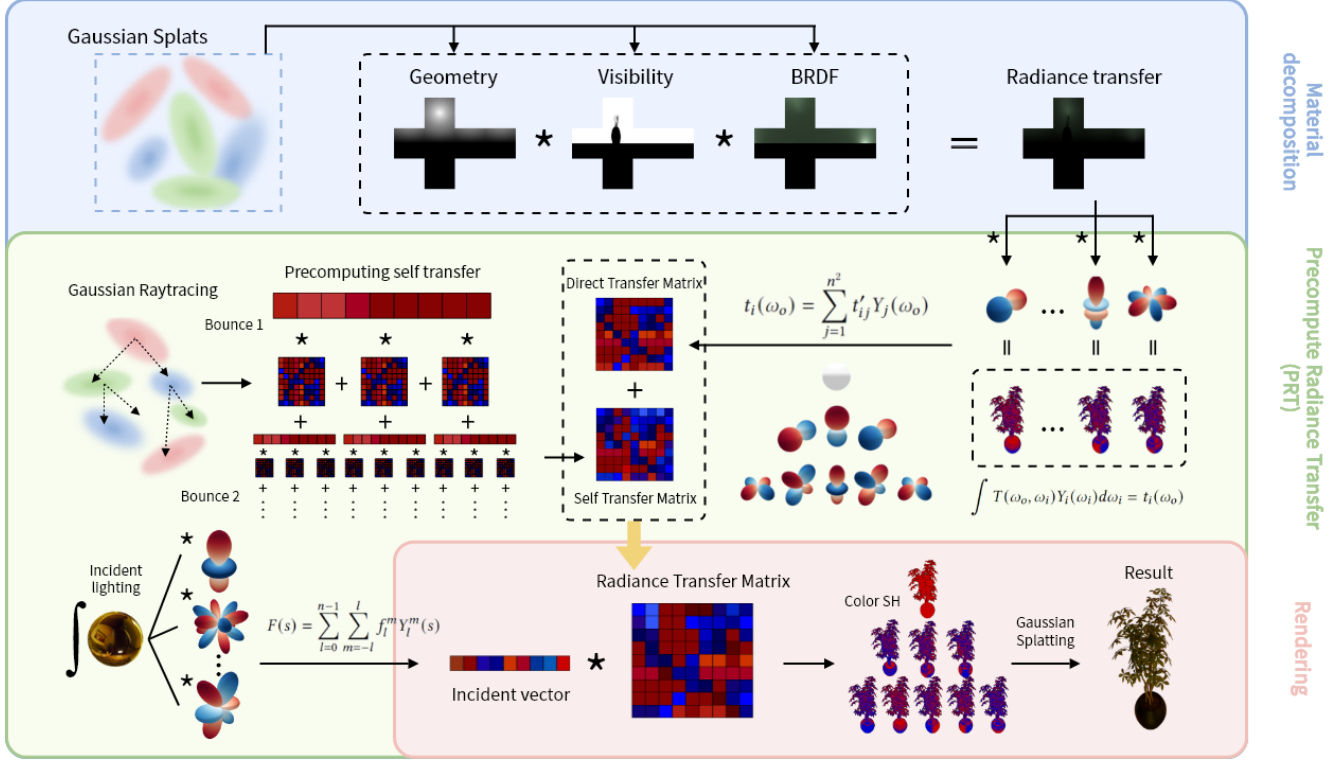


Figure 2: The proposed rendering pipeline. Starting with a collection of 3D Gaussian splats that embody geometry, visibility, and BRDF attributes along with incident lighting, we first compute the radiance transfer for every Gaussian splat by executing equation 28, the direct transfer matrix by equation 40 and the incident vector by equation 10. Following this, we conduct one-bounce 3D Gaussian ray tracing (Sec 4.4) to get the index matrix and precompute self-transfer for every Gaussian splat recursively to estimate indirect illumination based on the index matrix. Finally, we conduct a straightforward dot product between the radiance transfer matrix and incident vector in the spherical harmonics domain and compute the final rendering result with Gaussian splatting.

and

$$N = \sum_{i \in N} n_i \alpha_i \prod_{j=1}^{i-1} (1 - \alpha_j) \quad (25)$$

4.4 3D Gaussian Raytracing

In the context of 3D Gaussian splats, the computational overhead of ray tracing is notably increased. Because ray tracing cannot be initiated directly from screen space, multiple sampling is required for each Gaussian splat to achieve noise-free results. Moreover, rays need to bounce recursively between Gaussian splats, as the number of bounces increases, the computation for tracing and rendering grows exponentially with the sample amount. In this paper, we present a novel ray tracing technique integrated with self-transfer precomputation. Our approach streamlines the process by doing one-bounce ray tracing during the whole training or rendering stage and updating self-radiance transfer iteratively and recursively. As a result, we achieve precise computation of indirect illumination for multiple bounces under diverse dynamic environment lighting. Like [5, 7, 16], our proposed ray tracing technique on 3D Gaussian splats is constructed upon the Bounding Volume Hierarchy (BVH), facilitating efficient querying of visibility along a ray. Unlike conventional ray tracing methods, our approach does not involve computing irradiance during the ray tracing process.

Instead, we solely compute the weights W_i of the Gaussian splat intersected along each direction and record the index of the Gaussian splat with the maximum weight for each direction. Same as 4, our weight can be written as:

$$W_i = \alpha_i \prod_{j=1}^{i-1} (1 - \alpha_j) \max(-r_d \cdot n_i, 0) \quad (26)$$

where r_d is the normalized ray direction, n_i is the normal of hit Gaussian splat, and $\max(-r_d \cdot n_i, 0)$ prevents one Gaussian splat from being illuminated by the backside of another Gaussian splat. α_i is given by evaluating a 3D Gaussian splat with covariance Σ multiplied with a learned per-splat opacity.

$$\alpha_i = \frac{r_d^T \Sigma r_d}{r_d^T \Sigma r_d} \sigma_i \quad (27)$$

where σ_i is the opacity of hit Gaussian. To avoid illumination from other Gaussian splats on the same surface, we filter out all points when $\prod_{j=1}^{i-1} (1 - \alpha_j) > t$ and t is a hyperparameter that can be adjusted. Although we only performed one-bounce ray tracing, we can recursively compute n-bounce indirect illumination using equation 22, with minimal additional computational cost in terms of time. Please refer to section 4.5 for a detailed explanation of this. In summary, we performed one-bounce ray tracing in n directions

for each Gaussian splat and generated an index matrix. This matrix records the index of other Gaussian splats that exert the greatest contribution on the current Gaussian splat along n directions (if no splat is hit along a direction, it is recorded as -1). This index matrix is utilized to computing self-transfer. Note that we no longer update the positions and other geometric properties of Gaussian splats after ray tracing. Our training stage is performed on a set of stable Gaussian splats trained by using [11].

4.5 Precomputing Radiance Transfer for 3D Gaussian Splats

Transfer Vector for Training During training, it is necessary to iteratively update properties such as roughness and metallic for Gaussian splats. Consequently, radiance transfer for Gaussian splats needs to be computed in each iteration with a known view direction. However, iteratively computing the transfer matrix is costly. Therefore, we make a slight compromise on the accuracy of indirect illumination to substantially reduce training time. Given a view direction v , radiance transfer at Gaussian splat x can be rewritten as:

$$T(x, v, \omega_i) = (f_s(\omega_i, v) + f_d)(v \cdot n)V(v, x) \quad (28)$$

which is defined on sphere ω_i since v is given. According to equa-

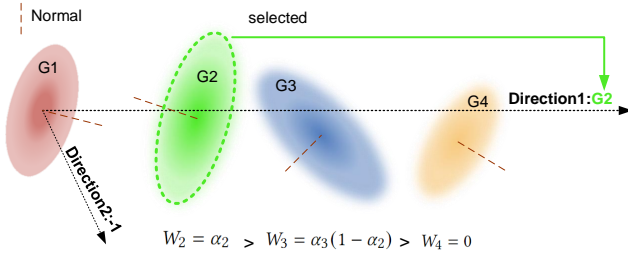


Figure 3: 3D Gaussian raytracing. Ray from G_1 at direction 1 hits 3 Gaussian splats G_2 , G_3 and G_4 , we compute the weight for each Gaussian splat by equation 26 and select the Gaussian splat with the biggest weight (G_2).

tion 11, we can simply precompute $T(x, \omega_i)$ into a transfer vector \vec{T} . However, the previously mentioned approach is not applicable for computing self-transfer. This is due to the inconsistency in the ω_o for interreflection, leading to exponentially increasing computational complexity. By assuming that all indirect illumination originates from diffuse surfaces, we can streamline complicated matrix calculations into vector calculations. Additionally, we precompute the diffuse radiance transfer:

$$T_{diffuse}(x, \omega_i) = f_d(\omega_i \cdot n)V(\omega_i, x) \quad (29)$$

into $\vec{T}_{diffuse}$. In sec 4.4, we precompute the index of other Gaussian splats x' that exert the greatest contribution on the current Gaussian splat along direction d_i . Therefore, we can quickly query its corresponding diffuse radiance transfer $\vec{T}_{diffuse}^{d_i}$. According to equation 22, one-bounce self-transfer can be written as:

$$T^1 = f(d_i, v)(d_i \cdot n) \int_{\Omega} T_{diffuse}^{d_i}(\omega_i^1, -d_i) d\omega_i^1 \quad (30)$$

and

$$T_{diffuse}^{d_i}(\omega_i^1) = \sum_{j=1}^{n^2} t_j Y_j(\omega_i^1) = \vec{T}_{diffuse}^{d_i} \cdot Y(\vec{\omega}_i^1) \quad (31)$$

then:

$$T^1 = \sum_{d_i} f(d_i, v)(d_i \cdot n) \vec{T}_{diffuse}^{d_i} \cdot Y(\vec{\omega}_i^1) \quad (32)$$

and one-bounce diffuse self-transfer can be written as:

$$T_{diffuse}^1 = \sum_{d_i} \frac{\rho}{\pi} (d_i \cdot n) \vec{T}_{diffuse}^{d_i} \cdot Y(\vec{\omega}_i^1) \quad (33)$$

Recursively, we can compute n -bounce self-transfer.

$$T^n = \sum_{d_i} f(d_i, v)(d_i \cdot n) \vec{T}_{diffuse}^{d_i, n-1} \cdot Y(\vec{\omega}_i^n) \quad (34)$$

Finally, the total self-transfer vector is:

$$\vec{T} = \sum_{j=1}^n \vec{T}^j \quad (35)$$

Although our method may not address specialized light paths (such as SDS path), it can efficiently compute simple specular interreflections (such as SD path) that [7, 16, 27] can't since current Gaussian splat is not assumed to be diffuse.

Transfer Matrix for unknown direction During relighting and other test tasks, we can precompute the transfer matrix for glossy cases since BRDF and other properties are certain. Given:

$$T(x, \omega_i, \omega_o) = (f_d + f_s(\omega_i, \omega_o))(\omega_i \cdot n)V(\omega_i, x) \quad (36)$$

According to equation 9, we have:

$$t_i(\omega_o) = \int T(\omega_o, \omega_i) Y_i(\omega_i) d\omega_i \quad (37)$$

$t_i(\omega_o)$ is defined on the sphere ω_o , so it can be represented as another set of basis functions:

$$t_i(\omega_o) = \sum_{j=1}^{n^2} t'_{ij} Y_j(\omega_o) \quad (38)$$

and $T(\omega_o, \omega_i)$ can be represented as:

$$T(\omega_o, \omega_i) = \sum_{i=1}^{m^2} \sum_{j=1}^{n^2} t'_{ij} Y_j(\omega_o) Y_i(\omega_i) \quad (39)$$

where:

$$t'_{ij} = \sum_{l=1}^q \sum_{k=1}^p Y_l(\omega_i^l) T(\omega_i^l, \omega_o^l) Y_j(\omega_o^k) \quad (40)$$

Here we sample ω_i m times and ω_o p times. Then equation 12 can be written as:

$$L_o(x) = \sum_{i=0}^{m^2} \sum_{j=0}^{n^2} l_i t'_{ij} = \vec{L} \cdot T_{m \times n} \quad (41)$$

Like 34, we can precompute self-transfer

However, we still opt for diffuse self-transfer in most cases due to its faster computation.

Table 1: Quantitative Comparison on TensorIR Synthetic Dataset. Our method outperforms both previous offline and real-time methods on Novel View Synthesis. Our relighting results rank first in all real-time methods and second in all methods, only behind TensorIR. Importantly, the average training time of our PRTGS is accelerated by a factor of 25 \times , and the average training time is accelerated by a factor of 10000 \times compared to TensorIR, making its performance acceptable and further demonstrating the effectiveness of our approach. The best results are marked in red, the second best are marked in blue.

Category	Method	Novel View Synthesis			Relighting			Render Time	Train Time
		PSNR \uparrow	SSIM \uparrow	LPIPS \downarrow	PSNR \uparrow	SSIM \uparrow	LPIPS \downarrow		
Offline	NeRFactor	24.740	0.916	0.114	23.606	0.902	0.122	>100s	4 days
	InvRender	25.879	0.928	0.088	22.754	0.892	0.104	63.49s	15 hours
	TensorIR	34.540	0.976	0.039	29.127	0.955	0.065	>100s	5 hours
RealTime	NVDiffrec	28.617	0.958	0.051	20.149	0.877	0.083	0.005s	1 hour
	Gsir	35.739	0.975	0.035	25.308	0.884	0.096	-	minutes
	Relightable	39.204	0.984	0.037	26.451	0.923	0.078	0.01s	minutes
	PRTGS (Ours)	41.985	0.988	0.022	28.964	0.952	0.068	0.015s	minutes



Figure 4: High-quality relighting results achieved by our proposed method on TensorIR dataset [9], DTU dataset [8] and a composite scene created by us.

5 EXPERIMENT

5.1 Implementation Details

Dataset and Metric We conduct experiments using benchmark datasets of TensorIR Synthetic [9], DTU [8] and Mipnerf-360 [3] to evaluate our method’s performance on both synthetic and real-world scene. We evaluate the synthesized novel view and relighting results in terms of Peak Signal-to-Noise Ratio (PSNR), Structural Similarity Index Measure (SSIM), and Learned Perceptual Image

Patch Similarity (LPIPS). **Baselines** Considering the popularity and performance, we selected NeRFactor [37], NeRFDiffRec [20], Invrender [38], TensorIR[9], Relightable 3DGS[7] and GSIR [16] as our main competitor. We conducted a comprehensive comparison between the aforementioned methods and our approach in terms of efficiency and quality. Our method are conducted on a single NVIDIA GeForce RTX 3090 GPU.

5.2 Results on Synthetic Datasets

We compare our method with previous state-of-the-art offline and real-time relighting methods. Table 1 shows that our method outperforms both previous offline and real-time methods on Novel view synthesis. Our relighting results rank first in all real-time methods and second in all methods, only behind TensoIR. Taking both efficiency and quality into account, our approach achieves optimality. Figure 4 shows visual results on Relighting tasks. We test our method under different lighting conditions and our method performs well on all lighting conditions with visually appearing results. Furthermore, we also test our method on composite synthetic scenes like [7] and the result shows that our method can not only facilitate material editing like [9, 16, 27] but also support scene editing and generate photo-realistic results and soft shadow.

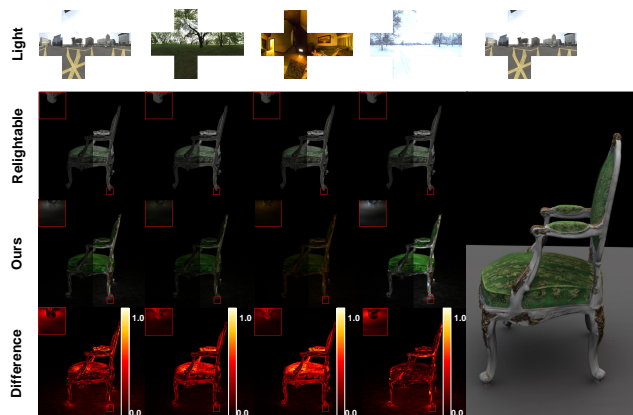


Figure 5: Qualitative comparison on TensoIR Synthetic dataset. We visualize the indirect illumination in different lighting conditions. To showcase more details, we have merged the doubled-scaled indirect illumination results (on the right half) with the original brightness indirect illumination results (on the left half). The top-left corner exhibits a magnified view of the local area.

Table 2: Quantitative Comparison on Mip-NeRF 360. Our method surpasses most NeRF variants and Gaussian inverse rendering method dedicated to novel view synthesis

Method	PSNR \uparrow	SSIM \uparrow	LPIPS \downarrow
NeRF++	26.214	0.659	0.348
Plenoxels	23.625	0.670	0.443
INGP-Base	26.430	0.725	0.339
Gsir	26.659	0.815	0.229
Ours	28.116	0.865	0.182

5.3 Results on real-world Datasets

We extend our evaluation to real-world dataset [3, 8] with geometric intricacies inherent and complex lighting conditions. Due to the lack of data under varying lighting conditions, Tab 2 only presents the quantitative comparisons on real-world datasets on Novel view synthesis tasks. From Tab 2 we can conclude that our real-time relighting approach even surpasses most NeRF variants and the

advanced inverse rendering method dedicated to novel view synthesis. Figure 4 demonstrates reconstructed scene details including high-frequency appearance, rendering high-fidelity appearance, and recovering fine geometric details.

5.4 Ablation

Indirect illumination To demonstrate the effectiveness of our indirect illumination model, we conducted comparisons with two alternative variants: a model without indirect illumination (w/o indirect) and a model with ambient occlusion indirect illumination (AO indirect). We report the average scores on the TensoIR dataset, as outlined in Tab 3. Our analysis reveals that accurate indirect illumination plays a pivotal role in estimating accurate material decomposition and producing photorealistic rendering results. To prove that our raytracing and indirect illumination estimation method can compute accurate indirect illumination related to environment light, we compare our method with Relightable 3DGS [7] in different lighting conditions. Figure 5 shows that the indirect illumination generated by our method not only adapts to lighting conditions but also adjusts with changes in the scene.

Table 3: Analyses on the impact of indirect illumination.

Method	TensoIR Synthetic			DTU		
	PSNR \uparrow	SSIM \uparrow	LPIPS \downarrow	PSNR \uparrow	SSIM \uparrow	LPIPS \downarrow
AO indirect	38.681	0.981	0.024	29.192	0.933	0.108
w/o indirect	39.122	0.983	0.022	29.301	0.934	0.108
Ours	41.985	0.988	0.022	29.458	0.935	0.107

Spherical Harmonics Order We investigate the impact of Spherical Harmonics Order on the relighting quality. We select orders 2, 3, and 6 and report the quantitative results on Tap 4. Our analysis indicates that under relatively smooth environmental lighting conditions, the order of spherical harmonic functions has a minor impact on the quality of results but a significant effect on rendering speed.

Table 4: Analyses on the impact of SH order. SH order has little influence on relighting quality.

Method	PSNR \uparrow	SSIM \uparrow	LPIPS \downarrow	Render time
SH Order 2	27.730	0.904	0.073	0.012
SH Order 3	27.722	0.904	0.073	0.013
SH Order 6	27.720	0.904	0.073	0.050

6 CONCLUSION

We proposed PRTGS, a real-time high-quality relighting method in low-frequency lighting environments for 3D Gaussian splatting. In terms of implementation, we precompute the expensive transport simulations required for complex transfer functions into sets of vectors or matrices for every Gaussian splat. We introduce distinct precomputing methods tailored for training and rendering stages, along with unique ray tracing and indirect lighting precomputation techniques for 3D Gaussian splats to accelerate training speed and compute accurate indirect lighting related to environmental light. Extensive experiments demonstrate the superior performance of our proposed method across multiple tasks, highlighting its efficacy and broad applicability in relighting, scene reconstruction, and editing.

REFERENCES

- [1] Dejan Azinovic, Tzu-Mao Li, Anton Kaplanyan, and Matthias Nießner. 2019. Inverse path tracing for joint material and lighting estimation. In *Proceedings of the IEEE/CVF Conference on Computer Vision and Pattern Recognition*. 2447–2456.
- [2] Jonathan T Barron, Ben Mildenhall, Matthew Tancik, Peter Hedman, Ricardo Martin-Brualla, and Pratul P Srinivasan. 2021. Mip-nerf: A multiscale representation for anti-aliasing neural radiance fields. In *Proceedings of the IEEE/CVF International Conference on Computer Vision*. 5855–5864.
- [3] Jonathan T. Barron, Ben Mildenhall, Dor Verbin, Pratul P. Srinivasan, and Peter Hedman. 2022. Mip-nerf 360: Unbounded anti-aliased neural radiance fields. In *Proceedings of the IEEE/CVF Conference on Computer Vision and Pattern Recognition*. 5470–5479.
- [4] Brent Burley and Walt Disney Animation Studios. 2012. Physically-based shading at disney. In *Acm Siggraph*, Vol. 2012. vol. 2012, 1–7.
- [5] Yiwen Chen, Zilong Chen, Chi Zhang, Feng Wang, Xiaofeng Yang, Yikai Wang, Zhongang Cai, Lei Yang, Huaping Liu, and Guosheng Lin. 2023. Gaussianeditor: Swift and controllable 3d editing with gaussian splatting. *arXiv preprint arXiv:2311.14521* (2023).
- [6] Sara Fridovich-Keil, Alex Yu, Matthew Tancik, Qinhong Chen, Benjamin Recht, and Angjoo Kanazawa. 2022. Plenoxels: Radiance fields without neural networks. In *Proceedings of the IEEE/CVF Conference on Computer Vision and Pattern Recognition*. 5501–5510.
- [7] Jian Gao, Chun Gu, Youtian Lin, Hao Zhu, Xun Cao, Li Zhang, and Yao Yao. 2023. Relightable 3d gaussian: Real-time point cloud relighting with brdf decomposition and ray tracing. *arXiv preprint arXiv:2311.16043* (2023).
- [8] Rasmus Jensen, Anders Dahl, George Vogiatzis, Engin Tola, and Henrik Aanaes. 2014. Large scale multi-view stereopsis evaluation. In *Proceedings of the IEEE conference on computer vision and pattern recognition*. 406–413.
- [9] Haian Jin, Isabella Liu, Peijia Xu, Xiaoshuai Zhang, Songfang Han, Sai Bi, Xiaowei Zhou, Zexiang Xu, and Hao Su. 2023. Tensor: Tensorial inverse rendering. In *Proceedings of the IEEE/CVF Conference on Computer Vision and Pattern Recognition*. 165–174.
- [10] James T Kajiya. 1986. The rendering equation. In *Proceedings of the 13th annual conference on Computer graphics and interactive techniques*. 143–150.
- [11] Bernhard Kerbl, Georgios Kopanas, Thomas Leimkühler, and George Drettakis. 2023. 3d gaussian splatting for real-time radiance field rendering. *ACM Transactions on Graphics* 42, 4 (2023), 1–14.
- [12] Anders Wang Kristensen, Tomas Akenine-Möller, and Henrik Wann Jensen. 2005. Precomputed local radiance transfer for real-time lighting design. In *ACM SIGGRAPH 2005 Papers*. 1208–1215.
- [13] Manuel Lagunas, Xin Sun, Jimei Yang, Ruben Villegas, Jianming Zhang, Zhixin Shu, Belen Masia, and Diego Gutierrez. 2021. Single-image full-body human relighting. *arXiv preprint arXiv:2107.07259* (2021).
- [14] Yue Li, Pablo Wiedemann, and Kenny Mitchell. 2019. Deep precomputed radiance transfer for deformable objects. *Proceedings of the ACM on Computer Graphics and Interactive Techniques* 2, 1 (2019), 1–16.
- [15] Zhengqi Li, Simon Niklaus, Noah Snavely, and Oliver Wang. 2021. Neural scene flow fields for space-time view synthesis of dynamic scenes. In *Proceedings of the IEEE/CVF Conference on Computer Vision and Pattern Recognition*. 6498–6508.
- [16] Zhihao Liang, Qi Zhang, Ying Feng, Ying Shan, and Kui Jia. 2023. Gs-ir: 3d gaussian splatting for inverse rendering. *arXiv preprint arXiv:2311.16473* (2023).
- [17] Xinguo Liu, Peter-Pike J Sloan, Heung-Yeung Shum, and John Snyder. 2004. All-Frequency Precomputed Radiance Transfer for Glossy Objects. *Rendering Techniques 2004* (2004).
- [18] Ben Mildenhall, Pratul P Srinivasan, Matthew Tancik, Jonathan T Barron, Ravi Ramamoorthi, and Ren Ng. 2021. Nerf: Representing scenes as neural radiance fields for view synthesis. *Commun. ACM* 65, 1 (2021), 99–106.
- [19] Thomas Müller, Alex Evans, Christoph Schied, and Alexander Keller. 2022. Instant neural graphics primitives with a multiresolution hash encoding. *ACM transactions on graphics (TOG)* 41, 4 (2022), 1–15.
- [20] Jacob Munkberg, Jon Hasselgren, Tianchang Shen, Jun Gao, Wenzheng Chen, Alex Evans, Thomas Müller, and Sanja Fidler. 2022. Extracting triangular 3d models, materials, and lighting from images. In *Proceedings of the IEEE/CVF Conference on Computer Vision and Pattern Recognition*. 8280–8290.
- [21] Minghao Pan, Rui Wang Xinguo Liu, Qunsheng Peng, and Hujun Bao. 2007. Precomputed radiance transfer field for rendering interreflections in dynamic scenes. In *Computer Graphics Forum*, Vol. 26. Wiley Online Library, 485–493.
- [22] Keunhong Park, Utkarsh Sinha, Jonathan T Barron, Sofien Bouaziz, Dan B Goldman, Steven M Seitz, and Ricardo Martin-Brualla. 2021. Nerfies: Deformable neural radiance fields. In *Proceedings of the IEEE/CVF International Conference on Computer Vision*. 5865–5874.
- [23] Albert Pumarola, Enric Corona, Gerard Pons-Moll, and Francesc Moreno-Noguer. 2021. D-nerf: Neural radiance fields for dynamic scenes. In *Proceedings of the IEEE/CVF Conference on Computer Vision and Pattern Recognition*. 10318–10327.
- [24] Gilles Rainer, Adrien Bousseau, Tobias Ritschel, and George Drettakis. 2022. Neural precomputed radiance transfer. In *Computer graphics forum*, Vol. 41. Wiley Online Library, 365–378.
- [25] Imari Sato, Yoichi Sato, and Katsushi Ikeuchi. 2003. Illumination from shadows. *IEEE Transactions on Pattern Analysis and Machine Intelligence* 25, 3 (2003), 290–300.
- [26] Yoichi Sato, Mark D Wheeler, and Katsushi Ikeuchi. 1997. Object shape and reflectance modeling from observation. In *Proceedings of the 24th annual conference on Computer graphics and interactive techniques*. 379–387.
- [27] Yahao Shi, Yanmin Wu, Chenming Wu, Xing Liu, Chen Zhao, Haocheng Feng, Jingtuo Liu, Liangjun Zhang, Jian Zhang, Bin Zhou, et al. 2023. Gir: 3d gaussian inverse rendering for relightable scene factorization. *arXiv preprint arXiv:2312.05133* (2023).
- [28] Peter-Pike Sloan, Jan Kautz, and John Snyder. 2002. Precomputed Radiance Transfer for Real-Time Rendering in Dynamic, Low-Frequency Lighting Environments. (2002).
- [29] Pratul P Srinivasan, Boyang Deng, Xiuming Zhang, Matthew Tancik, Ben Mildenhall, and Jonathan T Barron. 2021. Nerv: Neural reflectance and visibility fields for relighting and view synthesis. In *Proceedings of the IEEE/CVF Conference on Computer Vision and Pattern Recognition*. 7495–7504.
- [30] Guanjun Wu, Taoran Yi, Jiemin Fang, Lingxi Xie, Xiaopeng Zhang, Wei Wei, Wenyu Liu, Qi Tian, and Xinggang Wang. 2023. 4d gaussian splatting for real-time dynamic scene rendering. *arXiv preprint arXiv:2310.08528* (2023).
- [31] Zhiwen Yan, Chen Li, and Gim Hee Lee. 2023. Nerf-ds: Neural radiance fields for dynamic specular objects. In *Proceedings of the IEEE/CVF Conference on Computer Vision and Pattern Recognition*. 8285–8295.
- [32] Zeyu Yang, Hongye Yang, Zijie Pan, Xi Tian, and Li Zhang. 2023. Real-time photorealistic dynamic scene representation and rendering with 4d gaussian splatting. *arXiv preprint arXiv:2310.10642* (2023).
- [33] Yao Yao, Jingyang Zhang, Jingbo Liu, Yihang Qu, Tian Fang, David McKeenon, Yanghai Tsin, and Long Quan. 2022. Neif: Neural incident light field for physically-based material estimation. In *European Conference on Computer Vision*. Springer, 700–716.
- [34] Taoran Yi, Jiemin Fang, Guanjun Wu, Lingxi Xie, Xiaopeng Zhang, Wenyu Liu, Qi Tian, and Xinggang Wang. 2023. Gaussianreamer: Fast generation from text to 3d gaussian splatting with point cloud priors. *arXiv preprint arXiv:2310.08529* (2023).
- [35] Ye Yu and William AP Smith. 2019. Inverserendernet: Learning single image inverse rendering. In *Proceedings of the IEEE/CVF Conference on Computer Vision and Pattern Recognition*. 3155–3164.
- [36] Jingyang Zhang, Yao Yao, Shiwei Li, Jingbo Liu, Tian Fang, David McKeenon, Yanghai Tsin, and Long Quan. 2023. Neif++: Inter-reflectable light fields for geometry and material estimation. In *Proceedings of the IEEE/CVF International Conference on Computer Vision*. 3601–3610.
- [37] Xiuming Zhang, Pratul P Srinivasan, Boyang Deng, Paul Debevec, William T Freeman, and Jonathan T Barron. 2021. Nerfactor: Neural factorization of shape and reflectance under an unknown illumination. *ACM Transactions on Graphics (ToG)* 40, 6 (2021), 1–18.
- [38] Yuanqing Zhang, Jiaming Sun, Xingyi He, Huan Fu, Rongfei Jia, and Xiaowei Zhou. 2022. Modeling indirect illumination for inverse rendering. In *Proceedings of the IEEE/CVF Conference on Computer Vision and Pattern Recognition*. 18643–18652.